Journal of Coordination Chemistry

ISSN: 0095-8972 (Print) 1029-0389 (Online) Journal homepage: http://www.tandfonline.com/loi/gcoo20

Iron(II) complexes containing the 2,6-bis-iminopyridyl moiety. Synthesis, characterization, reactivity, and DNA binding

Shaban Y. Shaban, Nagi El-Shafai, Hanaa Mansour & Rudi Van Eldik

To cite this article: Shaban Y. Shaban, Nagi El-Shafai, Hanaa Mansour & Rudi Van Eldik (2015) Iron(II) complexes containing the 2,6-bis-iminopyridyl moiety. Synthesis, characterization, reactivity, and DNA binding, Journal of Coordination Chemistry, 68:12, 2054-2064, DOI: 10.1080/00958972.2015.1031656

To link to this article: http://dx.doi.org/10.1080/00958972.2015.1031656

Accepted author version posted online: 01 Apr 2015.
Published online: 13 Apr 2015.

Journal of Coordination Chemistry, 2015
Vol. 68, No. 12, 2054–2064, http://dx.doi.org/10.1080/00958972.2015.1031656

Iron(II) complexes containing the 2,6-bis-iminopyridyl moiety. Synthesis, characterization, reactivity, and DNA binding

SHABAN Y. SHABAN*†, NAGI EL-SHAFAI†, HANAA MANSOUR† and RUDI VAN ELDIK*‡§

†Chemistry Department, Faculty of Science, Kafrelsheikh University, Kafrelsheikh, Egypt
‡Department of Chemistry and Pharmacy, University of Erlangen-Nuremberg, Erlangen, Germany
§Faculty of Chemistry, Jagiellonian University, Krakow, Poland

(*Received 12 December 2014; accepted 11 March 2015*)

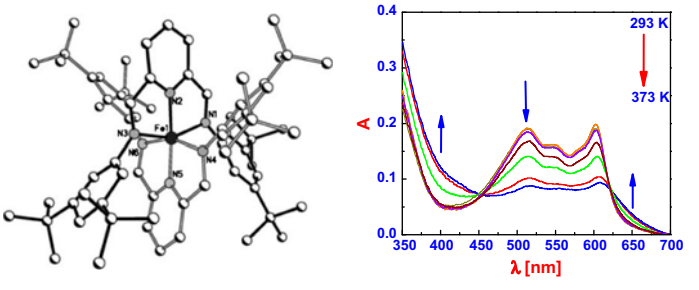

Two iron(II) complexes, $[Fe^{II}(py^tBuN_3)_2](FeCl_4)$ (**1**) and $[Fe^{II}(py^tBuMe_2N_3)Cl_2]$ (**2**), with sterically constrained py^tBuN_3 and $py^tBuMe_2N_3$ chelate ligands (py^tBuN_3 = 2,6-bis-(aldiimino)pyridyl; $py^tBuMe_2N_3$ = 2,6-bis-(ketimino)pyridyl), have been synthesized and characterized by elemental analysis, IR, UV–vis spectra, and preliminary X-ray single-crystal diffraction. The latter revealed that Fe(II) in **1** is six-coordinate by six nitrogen donors from two bisiminopyridines in a distorted octahedron. Complex **2** reacts with thiourea with a second-order rate constant $k_2 = (2.50 \pm 0.05) \times 10^{-3}$ M^{-1} s^{-1} at 296 K, and the reaction seemed to be slow. In a similar way, the interaction of **2** and DNA was studied by fluorescence and absorption spectroscopy. The results revealed that **2** caused fluorescence quenching of DNA through a dynamic quenching procedure. The binding constants K_A, K_{app}, and K_{SV} as well as the number of binding sites between **2** and DNA were determined.

Keywords: Fe(II) complexes; Spin transitions; DNA binding; Fluorescence spectra; Excitation

1. Introduction

The interaction of transition metal complexes with DNA have received attention over the past decade and became a hot topic owing to potential applications [1]. *Cis*-platin is widely used as an anticancer drug and the detailed molecular mechanism of its action involves

*Corresponding authors. Email: shaban.shaban@sci.kfs.edu.eg (S.Y. Shaban); Rudi.vanEldik@chemie.uni-erlangen.de (R. van Eldik)

covalent binding to DNA. However, *cis*-platin possesses inherent limitations such as high toxicity and low administration dosage [2]. Therefore, design and synthesis of systems that recognize specific sites of DNA is an important area in current research [3]. This could be at least in part due to formation of non-covalent association complexes by molecules containing nucleic acids. In many cases, such physical interaction may produce important pharmacological effects by interfering with the biological processes in which DNA/RNA take part. Sometimes such investigations also provide insight into the mechanism of action of naturally occurring antitumor antibiotics [4]. In this respect, there is a continued search for new metal complexes that strongly interact with DNA, and these studies led to the development of several new reagents [5].

In the past decade, interest in the chemistry of imine-based ligand systems has been revitalized by the discovery that their complexes may act as supporting ligands for a variety of excellent catalysts with a range of applications. The bis-imine pyridine ligand in particular has attracted considerable attention for its ability to provide unprecedented Ziegler–Natta catalysts based on late transition metals [6].

We report herein the synthesis, structure, and the DNA-binding studies of mono- and dinuclear iron(II) complexes containing bisimine ligands. No studies on the interaction of DNA with such complexes have yet been reported. The interaction was studied using UV–vis absorbance and fluorescence spectroscopy, and time-resolved fluorescence techniques.

2. Experimental

2.1. *General*

All chemicals used were of analytical reagent grade and of the highest purity commercially available. Iron(II) chloride dihydrate and pyridine-2,6-diacetyl (Aldrich) were used without further purification. Pyridine-2,6-dicarbaldehyde was synthesized as described in the literature [7]. 2,6-Bis-(aldimino)pyridine (**L1**) [8] and 2,6-bis-(ketimino)pyridine (**L2**) [9] were synthesized as reported previously.

2.2. *Synthesis*

2.2.1. Synthesis of $[Fe^{II}(py^{t}BuN_3)_2](FeCl_4)$ (1). $FeCl_2$ (38 mg, 0.3 mmol) was added to a suspension of 2,6-bis-(aldimino)pyridine (**L1**) (1.53 g, 0.3 mmol) in methanol and the mixture was stirred for 5 h. The resultant violet product was filtered off, washed with cold methanol (5 mL), and dried in vacuum to give **1** in 59% yield. Anal. Calcd for $C_{38}H_{22}Cl_4Fe_2N_6$ (816.12); Calcd: C, 55.92; H, 2.72; N, 10.30. Found: C, 55.30; H, 3.11; N, 11.01%. IR (KBr): ν, cm^{-1} = 3087 (s, C–H_{arom}), 2948 (s, C–H_{aliph}), 1620 (m, C=N); MS (FD^+, CH_3OH): m/z = 492 $[M]^+$.

2.2.2. Synthesis of $[Fe^{II}(py^{t}BuMe_2N_3)Cl_2]$ (2). $FeCl_2$ (35 mg, 0.3 mmol) was added to a suspension of 2,6-bis-(ketimino)pyridine (**L2**) (1.60 g, 0.3 mmol) in methanol and the mixture was stirred for 8 h. The resultant light violet solution was concentrated under vacuum and ether was added. The formed precipitate was filtered off, washed with ether (5 mL), and dried in vacuum to give **2** in 70% yield. Anal. Calcd for $C_{21}H_{15}Cl_2FeN_3$ (436.11);

Calcd: C, 57.83; H, 3.47; N, 9.64. Found: C, 58.30; H, 3.81; N, 9.98%. IR (KBr): ν, cm^{-1} = 3097 (s, C–H_{arom}), 2970 (s, C–H_{aliph}), 1630 (m, C=N); MS (FD^+, CH_3OH): m/z = 249 $[M - 2Cl]^+$.

2.3. *Instrumentation and measurements*

Spectra were recorded on the following instruments: IR (KBr disks, solvent bands were compensated): Mattson Infinity instrument (60 AR) at 4 cm^{-1} resolution from 400 to 4000 cm^{-1}; Mass spectra: Jeol MSTATION 700 spectrometer; Elemental analyses: Carlo Erba EA 1106 or 1108 analyzer.

Kinetic investigations on substitution reactions of the complexes by thiourea were performed either in tandem cuvettes with a path length of 0.88 cm, thermally equilibrated at 23 ± 0.1 °C before mixing, using a Varian Cary 1G spectrophotometer, or on *KinetAsyst* SF-61DX2 stopped-flow instrument (also thermostated at 23 ± 0.1 °C) with an optical pathlength of 1 cm at 394 nm. The temperature of the instruments was controlled with an accuracy of ± 0.1 °C. Thiourea was selected as entering nucleophile since its high nucleophilicity prevents the back reaction with chloride. The ligand substitution reactions were studied under pseudo-first-order conditions by using at least a 10-fold excess of thiourea. All listed rate constants represent an average value of at least three kinetic runs under each experimental condition.

2.4. *DNA-binding experiments*

Experimental work was carried out to investigate the interaction of the complexes with DNA.

2.4.1. Electronic absorption spectra. Electronic absorption spectroscopy is an efficient method to examine the binding mode of DNA to metal complexes. Concentrated stock solutions of the complex were prepared by dissolving it in tris–HCl buffer (pH 7.2) and carried out using a UV–visible Shimadzu 2450 spectrophotometer. A solution of calf thymus DNA (CT-DNA) in the buffer gave an UV absorbance at 260 nm, indicating that the DNA was sufficiently free of protein [10]. The concentration of the DNA was determined by absorption spectroscopy using the molar absorption coefficient (6600 M^{-1} cm^{-1}) at 260 nm [11]. Absorption titration experiments were carried out by varying the concentration of the CT-DNA while keeping the complex concentration constant at 1×10^{-4} M. The absorption spectra were measured with different concentrations of CT-DNA added to the complex solution. The spectral changes indicate that Fe-complex binds to DNA. The equilibrium for the DNA···Fe-complex can be given as shown by equation (1) for which the apparent association constant is given by equation (2).

$$\mathrm{DNA} + \mathrm{Fe-complex} \overset{K_{app}}{\rightarrow} \mathrm{Fe-complex \cdots DNA} \tag{1}$$

$$K_{app} = \frac{[\mathrm{BSA \cdots Fe-complex}]}{[\mathrm{BSA}][\mathrm{FE-complex}]} \tag{2}$$

The change in the absorption at 285 nm was utilized to obtain K_{app} according to the method reported by Benesi and Hildebrand [12] as expressed by equation (3):

$$\frac{1}{A_{obs} - A_0} = \frac{1}{A_c - A_0} + \frac{1}{K_{app}(A_c - A_0)[DNA]} \quad (3)$$

The relationship between $1/(A - A_0)$ *versus* reciprocal concentration of the DNA afforded a slope equal to $1/K_{app}(A_C - A_0)$ and an intercept equal to $1/(A_C - A_0)$ from which the apparent binding constant K_{app}, can be calculated.

2.4.2. Fluorescence quenching spectra. Fluorescence measurements were carried out on a Shimadzu RF-5301pc fluorescence spectrophotometer in a 1 cm path length quartz cell. The interaction of CT-DNA (1×10^{-4} M) with **2** was studied with the excitation and emission wavelength set at 285 nm. The intrinsic equilibrium binding constant (K_{sv}) was obtained by the linear Stern–Volmer equation (4) [13]:

$$I_0/I = 1 + K_q\tau_0[Q] = 1 + K_{sv}[Q] \quad (4)$$

where I_0 and I represent the fluorescence intensities in the absence and presence of quencher, respectively, K_q is the quenching rate constant of the biomolecule, K_{SV} the dynamic quenching constant, τ_0 the average lifetime of the biomolecule without quencher, and $[Q]$ the concentration of quencher. The set of data fitted to equation (4) gives a slope K_{sv}.

3. Results and discussion

L1 and **L2** with different substituents in the imino position of the bridge were synthesized according to the procedure described previously [8, 9]. Addition of one equivalent of pyridine-2,6-dicarbaldehyde or pyridine-2,6-diacetylpyridine to two equivalents of 3,5-di-*tert*-butylaniline in methanol yields the target ligands **L1** and **L2**, respectively. We prepared two iron(II) complexes (**1** and **2**) with **L1** and **L2** by treating the respective ligand (1 equiv.) with $FeCl_2$ in methanol under reflux (scheme 1; see the Experimental Section for details). The complexes were obtained as purple solids in moderate yields. Complexes **1** and **2** were characterized by elemental analysis, IR spectroscopy, and mass spectroscopy as applicable. The elemental analyses confirmed that the isolated complexes were in accord with the formulas $[Fe^{II}(py^tBuN_3)_2](FeCl_4)$ and $[Fe^{II}(py^tBuMe_2N_3)Cl_2]$ for **1** and **2**, respectively. The IR spectra of **L1** and **L2** show C=N stretches at 1626 and 1620 cm^{-1}, respectively. In **1** and **2**, the C=N stretches shift to lower frequency at 1612 and 1604 cm^{-1}, respectively. This is a further indication for the interaction between the imino nitrogens and the iron center.

A preliminary structure of $[Fe^{II}(py^tBuN_3)_2](FeCl_4)$ (**1**) was determined by X-ray crystallography. It proved to be very difficult to obtain suitable single crystals for **1**. A number of attempted structure determinations always resulted in high residual electron density maxima close to the two central iron ions, and showed the presence of numerous solvent molecules. However, the overall connectivity and geometry of $[\mathbf{1}](FeCl_4)$ could be established (figure 1). Complex $[\mathbf{1}](FeCl_4)$ has the iron ion in a pseudo-octahedral

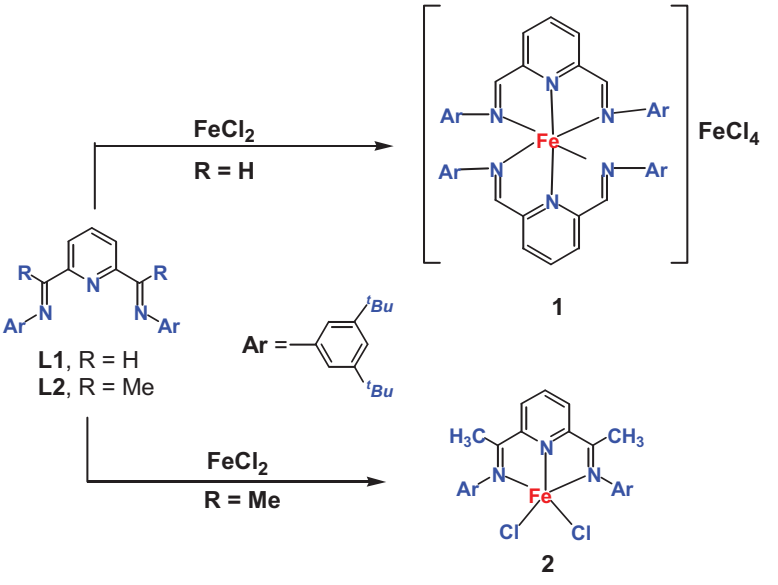

Scheme 1. Synthesis of **1** and **2**.

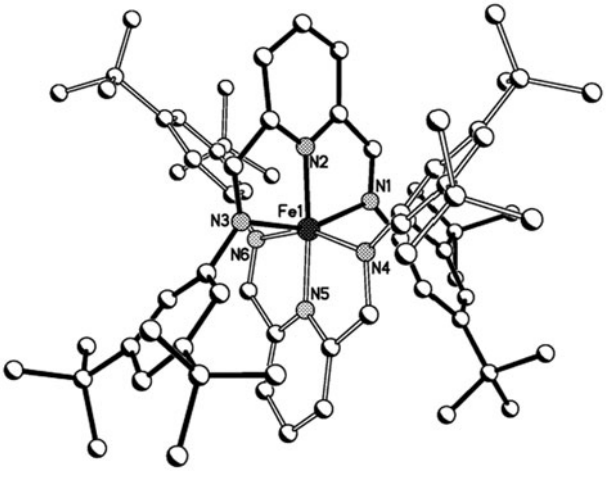

Figure 1. The overall connectivity and geometry of the cation [**1**]($FeCl_4$) as obtained from a preliminary X-ray structure determination.

coordination environment, as set up by the two essentially orthogonal tridentate nitrogen ligands. The structural data are in accord with those found in related iron(II) complexes [14].

3.1. *Kinetic studies on ligand substitution*

The earlier reported studies on DNA-binding models demonstrated that the exchange or interaction between the model complexes with a good leaving group incorporated in the complex initiated the binding or interaction. If the coordinating groups are stronger ligands

than DNA, no binding will be observed for the model complexes. To further elucidate the binding activity of the reported models **1** and **2**, a detailed kinetic study on ligand substitution was performed. Thiourea was selected as entering nucleophile because of its high nucleophilicity. Furthermore, it was selected as a neutral entering ligand such that the overall reaction is accompanied by charge creation, and the formation of the transition state may involve changes in dipole moment which will affect the activation parameters.

Reactions with thiourea can be monitored kinetically from 360 to 400 nm. Solutions were prepared by dissolving known amounts of **1** and **2** in methanol. The substitution reactions were studied as a function of TU concentration. Complex **1** did not show any substitution reaction with thiourea. UV/Vis spectral changes and representative kinetic traces for **2** are shown in figure 2.

Rate constant for the reaction of **2** with TU was determined by using total TU concentrations in the range 0.001–1.0 M, i.e. always at least in 10-fold excess over the iron(II) complex. Throughout the nucleophile concentration range, it was possible to fit the absorbance/time traces to a single-exponential function by using the following equation:

$$A = a_1 e^{-k_{\text{obsd1}} t} + A_0 \tag{5}$$

The overall monophasic reaction can be accounted for in terms of a single-substitution reaction [equation (6)] in which the chloride is displaced by TU characterized by the second-order rate constant $k_2 = (2.50 \pm 0.05) \times 10^{-3}\ \text{M}^{-1}\ \text{s}^{-1}$, indicating that the reaction is slow. It follows that k_{obs} should depend linearly on the entering TU concentration in the absence of a back reaction as shown in figure 3 such that $k_{\text{obs}} = k_2[\text{Nu}]$.

$$[\text{Fe(L)(Cl)}_2]^0 + \text{TU} \xrightarrow{k_2} [\text{Fe(L)(Cl)(TU)}]^+ + \text{Cl}^- \tag{6}$$

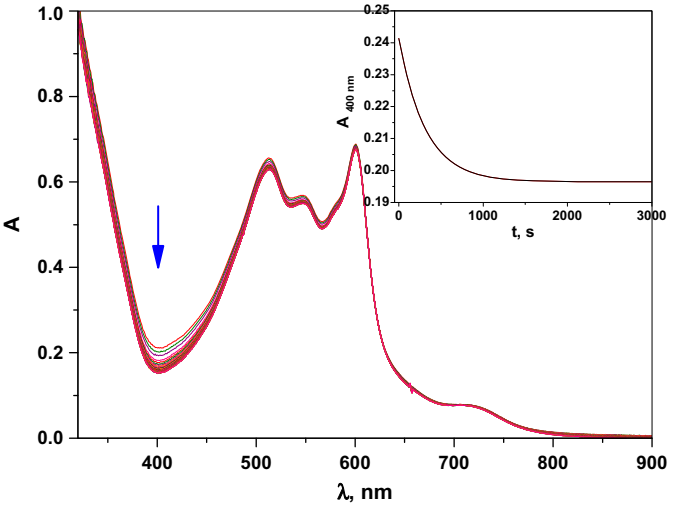

Figure 2. UV/Vis spectral changes recorded for the reaction of **2** (0.5×10^{-4} M) with thiourea (250 mmol) in methanol at 296 K. Inset is the absorbance time trace at 400 nm for the reaction measured by stopped-flow (solid line obtained by fitting the data with a single-exponential function according to equation 5).

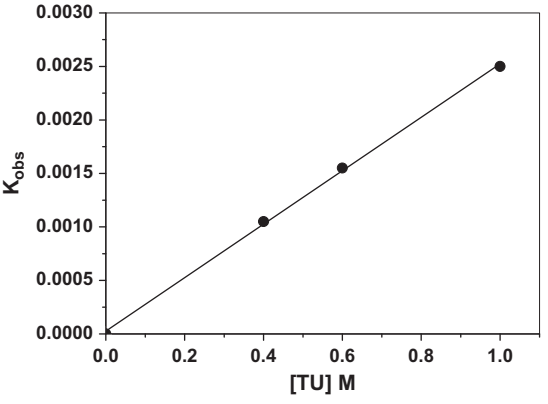

Figure 3. Plot of k_{obs} *vs.* thiourea concentration for **2** in methanol at 296 K. Experimental conditions: [**2**] = 0.5 × 10^{-4} M.

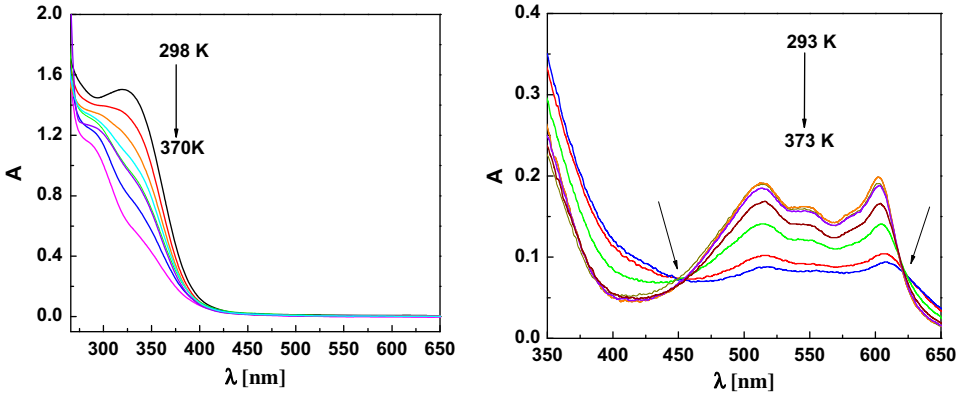

Figure 4. Temperature-dependent UV/Vis spectra of a solution of **1** (left) and **2** (right) in DMSO ([complex] = 1.4 × 10^{-4} M; 10 K intervals between 293 and 373 K).

3.2. *Electronic spectroscopy*

Figure 4 shows the electronic absorption spectra of solutions of **1** and **2** in DMSO at 293 K. Both complexes have strong absorption bands in the UV region, attributed to ligand-centered π–π^* and n–π^* transitions. Complex **2** shows two moderate bands in the visible region, characteristic of metal-to-ligand charge transfer (MLCT) transitions. In view of the structures of the present ligands, we assume this transition to give rise to the maximum absorbance bands in the 600–610 nm range of the UV/Vis spectra. The second MLCT band in the range of 500–520 nm may be due to a transition to a low-lying macrocycle-based LUMO + 1 in the ligand [14b].

Spin transitions of transition-metal complexes always give rise to pronounced thermochromism, which in the case of iron(II) complexes is often accompanied by bleaching of

the MLCT absorption bands [15]. Accordingly, our complex shows extensive bleaching of the typical MLCT absorption bands at 480–620 nm at elevated temperatures. Solutions of **2** in DMSO changed from blue at room temperature to almost colorless at 373 K.

Besides the monotonous bleaching of the MLCT transition, heating also causes significant spectral dynamics below 400 nm (intraligand absorptions; figure 4) which are characterized by well-defined isosbestic points. The appearance and the temperature dependence of the intraligand transitions in the UV/Vis spectra of **1** strongly resemble those of **2**. In particular, the isosbestic point at 445 nm is observed in both cases. The strong spectral parallel between **2** and **1** favors the possibility of a common molecular origin of the spectral dynamics and is compatible with the presence of spin equilibria in solution [16].

3.3. *Fluorescence quenching spectra*

The fluorescence intensity can be quenched by the addition of another molecule due to decrease in the binding sites of DNA [17]. Fluorescent quenching can occur in two different mechanisms, static quenching and dynamic quenching. For dynamic quenching, the mechanism can be described by the Stern–Volmer equation (4). In order to confirm the quenching mechanism, the procedure of the fluorescence quenching was first assumed to be a dynamic quenching process. Figure 5 displays the Stern–Volmer plots of the quenching of the fluorescence of **2** by DNA at room temperature. The corresponding quenching constants for the interaction between **2** and DNA was $K_{SV} = 1.31 \times 10^2$. When the fluorescence lifetime of the biopolymer is taken as 10^{-8} s [18], the quenching rate constant K_q was calculated to be 1.3×10^{10} L mol^{-1} s^{-1}. According to the literature for dynamic quenching [19], the maximum scatter collision quenching constant of various quenchers with biopolymers is 2.0×10^{10} L mol^{-1} s^{-1}. This means that the rate constant for the quenching of DNA by **2** nearly equals the K_q of the scatter procedure and the quenching therefore probably occurs via dynamic collision.

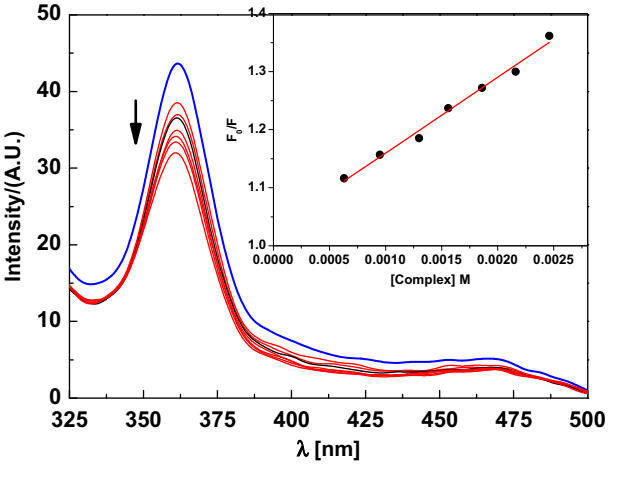

Figure 5. Fluorescence quenching of DNA (1×10^{-4}) in the absence (red) and presence (violet) of **2** in the concentration range of (6–24) $\times 10^{-4}$ M (at increments of 3 equiv). Inset is the Stern–Volmer plot for the steady-state fluorescence quenching of DNA by **2** (see http://dx.doi.org/10.1080/00958972.2015.1031656 for color version).

3.4. *UV–vis absorption spectra for DNA binding*

Complex **1** does not show any spectral changes and was almost inert, whereas the absorption spectra of **2** showed significant changes on increasing the concentration of CT-DNA as shown in figure 6. It can be seen from figure 5 that the Stern–Volmer plot does not show a significant deviation toward the *y*-axis in the experimental concentration range, which is an indication that either dynamic quenching or static quenching is predominant. In order to validate the dynamic quenching mechanism, the UV–vis absorption spectra of **2** and DNA were measured. Figure 6 shows that the peak of **2** around 285 nm is not red- or blue-shifted and the maximum absorption wavelength increases after addition of appropriate amounts of DNA, indicating that the interaction between **2** and DNA is dynamic. The linear relationship between $1/(A - A_0)$ and the reciprocal concentration of DNA has a slope equal to $1/K_{app}(A_C - A_0)$ and an intercept equal to $1/(A_C - A_0)$ as shown in figure 6. The resulting apparent binding constant, K_{app}, is 1.69 M^{-1}.

3.5. *Binding constant and binding sites*

In order to obtain more detailed information on the mechanism of quenching and to further support the dynamic quenching, a static quenching model was studied. For static quenching, the relationship between fluorescence quenching intensity and the concentration of quencher can be described by equation (7) [20]:

$$\log\frac{F_0 - F}{F} = \log K_A + n\log[Q] \tag{7}$$

where K_A is the binding constant and n is the number of binding sites per DNA. After the fluorescence quenching intensities on DNA at 285 nm were measured, the double logarithm

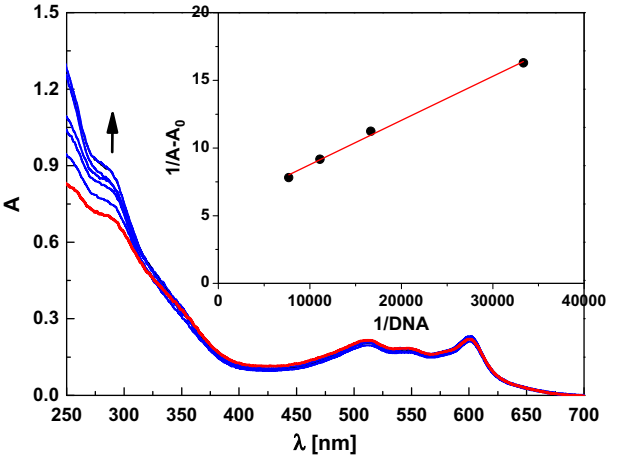

Figure 6. Absorption spectra of **2** (1.0×10^{-4} M) recorded in the absence (red) and presence (violet) of different concentrations of DNA as monitored by ultraviolet/visible spectroscopy. Inset is the plot of $\frac{1}{A-A_0}$ *vs.* $\frac{1}{[DNA]}$ at 285 nm as a function of number of Fe-complex equivalents (see http://dx.doi.org/10.1080/00958972.2015.1031656 for color version).

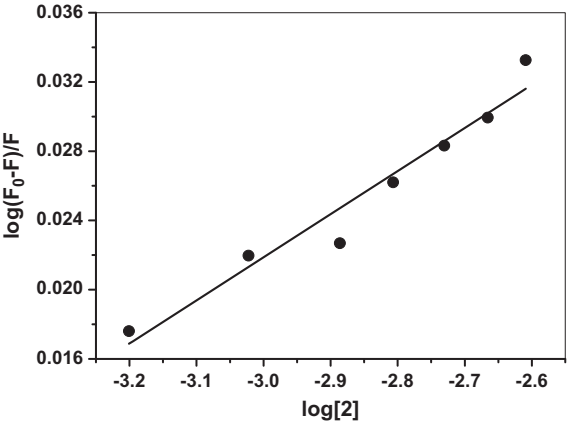

Figure 7. Plot of $\log\frac{F_0-F}{F}$ *vs.* log[**2**].

algorithm was assessed by equation (7). Figure 7 shows the double logarithm plot of log $(F_0 - F)/F$ *versus* log[**2**]. The correlation coefficients are larger than 0.94, indicating that the interaction between DNA and **2** does not agree well with the site-binding model underlined by equation (7) and support the dynamic quenching mechanism. Also, the number of binding sites ($n = 0.03$) and the binding constant (1.3 mol^{-1} L) support this type of mechanism.

4. Conclusion

The synthesis, characterization, and temperature-dependent UV–vis spectra of the iron(II) complexes $[Fe^{II}(py^tBuN_3)_2](FeCl_4)$ (**1**) and $[Fe^{II}(py^tBuMe_2N_3)Cl_2]$ (**2**) are reported. Complex **1** does not show any substitution as well as DNA-binding reaction, whereas **2** shows both reactions. Complex **1**, as shown from preliminary X-ray crystallography, is in a close proximity of two ligand moieties that block the coordination cavities. Fluorescence and absorption spectroscopy methods for determination of the interaction between **2** and DNA were provided. The results give preliminary information on the binding of **2** to DNA and dynamic quenching is confirmed to result in the observed fluorescence quenching.

Acknowledgements

Assistance with the preliminary X-ray crystal structure analysis and helpful discussion with Dr F.W. Heinemann, University of Erlangen-Nuremberg, Germany, and financial support from the Deutsche Forschungsgemeinschaft are gratefully acknowledged.

Disclosure statement

No potential conflict of interest was reported by the authors.

References

[1] (a) J.K. Barton, A. Danishefsky, J. Goldberg. *J. Am. Chem. Soc.*, **106**, 2172 (1984); (b) J.K. Barton, E.D. Olmon, P.A. Sontz. *Coord. Chem. Rev.*, **255**, 619 (2011); (c) Y. Jenkins, A.E. Friedman, N.J. Turro, J.K. Barton. *Biochemistry*, **31**, 10809 (1992); (d) A.E. Friedman, J.C. Chambron, J.P. Sauvage, N.J. Turro, J.K. Barton. *J. Am. Chem. Soc.*, **112**, 4960 (1990); (e) P. Uma Maheswari, M. Palaniandavar. *J. Inorg. Biochem.*, **98**, 219 (2004); (f) C.J. Burrows, J.G. Muller. *Chem. Rev.*, **98**, 1109 (1998); (g) G. Natile, M. Coluccia. *Coord. Chem. Rev.*, **216–217**, 383 (2001); (h) H. Chen, J.A. Parkinson, S. Parsons, R.A. Coxall, R.O. Gould, P.J. Sadler. *J. Am. Chem. Soc.*, **124**, 3064 (2002).

[2] (a) Y.B. Zeng, N. Yang, W.S. Liu, N. Tang. *J. Inorg. Biochem.*, **97**, 258 (2003); (b) B. Rosenberg, L. Van Camp, J.E. Trosko, V.H. Mansour. *Nature*, **222**, 385 (1969); (c) E.R. Jamieson, S.J. Lippard. *Chem. Rev.*, **99**, 2467 (1999); (d) E. Wong, C.M. Giandomenico. *Chem. Rev.*, **99**, 2451 (1999).

[3] (a) D.S. Sigman, T.W. Bruice, A. Mazumder, C.L. Sutton. *Acc. Chem. Res.*, **26**, 98 (1993); (b) J.K. Barton, A.M. Pyle. *Prog. Inorg. Chem.*, **38**, 413 (1990); (c) A.M. Burkhoff, T.D. Tullius. *Nature*, **331**, 455 (1988); (d) C.G. Riordan, P.J. Wei. *J. Am. Chem. Soc.*, **116**, 2189 (1992); (e) I. Meistermann, V. Moreno, M.J. Prieto, E. Molderheim, E. Sletten, S. Khalid, P.M. Rodger, M.J. Hannon. *Proc. Natl. Acad. Sci. USA*, **99**, 5069 (2002).

[4] (a) J.D. Tan, S.E. Hudson, S.J. Brown, M.M. Olmstead, P.K. Mascharak. *J. Am. Chem. Soc.*, **114**, 3841 (1992); (b) K. Nagai, B.J. Carter, J. Xu, S.M. Hecht. *J. Am. Chem. Soc.*, **113**, 5099 (1991); (c) K.C. Nicolau, P. Maligres, J. Shin, E. de Leon, D. Rideout. *J. Am. Chem. Soc.*, **114**, 7825 (1992).

[5] S.S. Mandal, U. Varshney, S. Bhattacharya. *Bioconjugate Chem.*, **8**, 798 (1997).

[6] J. Scott, S. Gambarotta, I. Korobkov, Q. Knijnenburg, B. de Bruin, P.H.M. Budzelaar. *J. Am. Chem. Soc.*, **127**, 17204 (2005), and references therein.

[7] N.W. Alcock, R.G. Kingston, P. Moore, C. Pierpoint. *J. Chem. Soc., Dalton Trans.*, 1937 (1984).

[8] S.Y. Shaban, F.W. Heinemann, R. van Eldik. *Eur. J. Inorg. Chem.*, 3111 (2009).

[9] S.Y. Shaban, A.M. Ramadan, R. van Eldik. *J. Coord. Chem.*, **65**, 2415 (2012).

[10] S. Satyanarayana, J.C. Dabrowiak, J.B. Chaires. *Biochemistry*, **32**, 2573 (1993).

[11] M. Reichmann, S. Rice, C. Thomas, P. Doty. *J. Am. Chem. Soc.*, **76**, 3047 (1954).

[12] H.A. Benesi, J.H. Hildebrand. *J. Am. Chem. Soc.*, **71**, 2703 (1949).

[13] O. Stern, M. Volmer. *Z. Phys.*, **20**, 183 (1919).

[14] (a) S.K. Hain, F.W. Heinemann, K. Gieb, P. Müller, G. Hörner, A. Grohmann. *Eur. J. Inorg. Chem.*, 187 (2010); (b) E.A. Medlycott, G.S. Hanan, T.S.M. Abedin, L.K. Thompson. *Polyhedron*, **27**, 493 (2008).

[15] (a) U. El-Ayaan, F. Murata, Y. Fukuda. *Monatsh. Chem.*, **132**, 1279 (2001); (b) P. Gütlich, H.A. Goodwin. *Top. Curr. Chem.*, **233**, 1 (2004).

[16] S. Schenker, P.C. Stein, J.A. Wolny, C. Brady, J.J. McGarvey, H. Toftlund, A. Hauser. *Inorg. Chem.*, **40**, 134 (2001).

[17] K. Dhara, P. Roy, J. Ratha, M. Manassero, P. Banerjee. *Polyhedron*, **26**, 4509 (2007).

[18] (a) J.R. Lakowicz, G. Weber. *Biochemistry*, **12**, 4161 (1973); (b) H. Xu, Q. Liu, Y. Wen. *Spectrochim. Acta, Part A*, **71**, 984 (2008).

[19] (a) Y.J. Hu, Y. Liu, L.X. Zhang, R.M. Zhao, S.S. Qu. *J. Mol. Struct.*, **750**, 174 (2005); (b) Y.M. Liu, G.Z. Li, X.F. Sun. *Chin. J. Anal. Chem.*, **32**, 615 (2004).

[20] (a) X.Z. Feng, R.X. Jin, Y. Qu, X.W. He. *Chem. J. Chin. Univ.*, **17**, 866 (1996); (b) X.F. Wei, H.Z. Liu. *Chin. J. Anal. Chem.*, **28**, 699 (2000).